Materials Letters 293 (2021) 129681

Contents lists available at ScienceDirect

Materials Letters

journal homepage: www.elsevier.com/locate/mlblue

Tailoring the photoluminescence of $BaMoO_4$ and $BaWO_4$ hierarchical architectures via precipitation induced by a fast precursor injection

Wyllamanney da S. Pereira, Júlio C. Sczancoski *, Elson Longo

Universidade Federal de São Carlos, Department of Chemistry, São Carlos SP, Brazil

ARTICLE INFO

Article history:
Received 12 January 2021
Received in revised form 5 March 2021
Accepted 6 March 2021
Available online 14 March 2021

Keywords:
Crystal growth
Photoluminescence
Tungstates
Molybdates

ABSTRACT

We investigate the effects of temperature and reaction time on structural, morphological, and optical properties of $BaMoO_4$ and $BaWO_4$ synthesized via precipitation induced by a fast precursor injection. Oriented aggregation and matter transfer influenced the particle sizes and shapes. The morphological changes were responsible for manipulating the maximum photoluminescence (PL) emissions from blue to red, exclusively in $BaWO_4$. The broadband PL profiles and band gap energies (from 4.08 to 4.98 eV) suggested the participation of direct electronic transitions among intermediary energy levels in the forbidden region. The proposed template/surfactant-free approach has the potential to growth hierarchical structures of tungstates/molybdates with improved optical properties.

1. Introduction

The crystallization of inorganic particles with controlled shapes and sizes is a great challenge to design new functionalities in materials. Many efforts have been devoted to understanding the growth dynamics of hierarchical architectures (HAs). HAs are based on the self-assembly of inorganic building blocks over multiple length scales [1], which have been seen in a variety of tungstates/molybdates [2].

The interest in scheelites is centered on developing scintillators, light-emitting diodes, and solid-state lasers [3]. The key to such technological applications is the intrinsic luminescence of these phosphors. As excellent host matrices, depending on the incorporated element and excitation wavelength, the luminescence can be improved [4]. However, few studies have shown how to tune the photoluminescence (PL) properties in single-phase scheelites via morphological control.

The precipitation-based routes are very promising among the diverse preparation methods because of their technical simplicity, versatility, and scalable production. Thus, researches aiming at the precipitation of barium molybdate ($BaMoO_4$) and barium tungstate ($BaWO_4$) have been limited to the instantaneous reaction at room temperature with/without post-heat treatments [5].

In our study, $BaMoO_4$ and $BaWO_4$ were synthesized via precipitation induced by a fast precursor injection (P-FPI). The purpose was to explore the role of different reaction times in the morphological features and PL response of these phosphors.

2. Materials and methods

2.1. Synthesis

Sodium molybdate dihydrate ($Na_2MoO_4{\cdot}2H_2O$, 99.5%), sodium tungstate dihydrate ($Na_2WO_4{\cdot}2H_2O$, 99%), and barium nitrate ($Ba(NO_3)_2$, 99%) were purchased from Sigma-Aldrich. For the synthesis of $BaMoO_4$ at 90 °C, 4 mmol of $Na_2MoO_4{\cdot}2H_2O$ and $Ba(NO_3)_2$ were dissolved in 20 and 80 mL of deionized water, respectively. The first solution (Na^+ and MoO_4^{2-} ions) maintained at room temperature was sucked with a syringe and quickly injected into the other (Ba^+ ions) heated at 90 °C into an angled two-neck round bottom flask coupled to a reflux condenser with thermostatic bath. After precipitation, this system was maintained at 90 °C for different times. The obtained products were centrifuged, washed with deionized water/acetone, and dried at 60 °C for 2 h. A similar procedure was adopted for $BaWO_4$. The reaction time referred to as 0 h corresponds to instantaneously precipitated samples at 30 or 90 °C. The samples prepared at 30 °C for 0 h were chosen to analyze the influence of temperature.

2.2. Characterization

X-ray diffraction (XRD) patterns were recorded on an XRD-6000 diffractometer (Shimadzu) with CuKα radiation (λ = 0.154184 nm)

* Corresponding author.
E-mail address: jcsfisica@gmail.com (J.C. Sczancoski).

https://doi.org/10.1016/j.matlet.2021.129681
0167-577X/

by using a scanning scan rate and step size of 1°/min and 0.02°, respectively. Raman spectra were analyzed on a RF-100 FT-Raman spectrometer (Bruker Optik) equipped with an Nd:YAG laser (λ = 532 nm) operating at 100 mW. The morphological aspects were verified on a SUPRA 35VP scanning electron microscope (SEM) (Carl Zeiss). Ultraviolet–Visible (UV–Vis) spectra were taken on a Cary 5G spectrophotometer (Varian) operating in diffuse reflectance mode. PL spectra at room temperature were performed on a Monospec-27 monochromator (Thermal Jarrel-Ash) coupled to an R446 photomultiplier (Hamamatsu Photonics). The excitation wavelength was a Kr-ion laser (λ = 350 nm) (Coherent Innova 90 K) with the maximum power at 15 mW.

3. Results and discussion

The high crystallinity is a fingerprint of the scheelites, even in production methods performed at 30 °C [2]. Such feature was identified in the diffractograms of $BaMoO_4$ and $BaWO_4$ with scheelite-type tetragonal structures (JCPDS 29–0193 and 43–0646) (Fig. S1 in Supplementary Data (SD)). To enrich this information, Raman spectra (Fig. S2) presented well-defined bands arising from anti-symmetric and symmetric vibrational frequencies of $[MoO_4]$ or $[WO_4]$ and $[BaO_8]$ clusters [6].

Analyzing the morphology, the samples synthesized at 30 °C exhibited several rice-like microparticles containing rugged defects (Fig. 1a and 2a). By increasing both temperature (from 30 to 90 °C) and reaction time, the growth of shuttle-like microparticles (Fig. 1b-f and 2b-f) with an average particle size from 12 to 41 μm (Figs. S3 and S4) was observed. These HAs were organized by repeated edge-to-edge attachments of flattened and faceted particles along the ⟨001⟩ direction with four branches (truncated bipyramidal particles) perpendicular to the central axis [2]. The oriented attachment process accompanied by the appearance of defects is indicative of a non-classical crystallization mechanism [7].Fig. 2.

SEM images showed that the evolution in the reaction time provoked surface changes in shuttle-like microparticles. Many damaged particles were seen in the syntheses performed for 12 and 24 h, as well as some internally hollow $BaMoO_4$ microparticles (Insets in Fig. 1c-e). Two hypotheses were assumed for the observed phenomena: (i) diffusion of precursor molecules/ions from solution to surface; (ii) matter transfer from bulk to surface. When the $BaMoO_4$ and $BaWO_4$ were compared (Fig. S5), the slight modifications in particle shapes were assigned to intrinsic differences in the bonding environmental of $[MoO_4]$ and $[WO_4]$ clusters during the nucleation/growth stages.

The band gap energies (E_{gap}) were estimated via UV–Vis spectroscopy by the Kubelka-Munk method for direct transitions [8,9]. The E_{gap} results were found from 4.08 to 4.21 eV in $BaMoO_4$ and from 4.87 to 4.98 eV in $BaWO_4$ (Figs. S6 and S7). More details on these results in SD. When excited at 350 nm (3.54 eV), broadband PL spectra with the maximum emission peaks were detected from 468 nm (2.65 eV) to 507 nm (2.44 eV) in $BaMoO_4$, and from 474 nm (2.61 eV) to 578 nm (2.14 eV) in $BaWO_4$ (Figs. 3 and 4). As the excitation energy was lower than the E_{gap} in both phosphors, PL emissions arose from charge transfer transitions involving intermediary energy levels (IEL) in the band gap. Defects were responsible for the creation of such IEL, commonly labeled as shallow-level defect states (SLS) and deep-level defect states (DLS) [10].

Broadband PL profiles are originated from the contribution of multicolor visible emissions with distinct wavelengths. Mathematical functions are an acceptable approach to qualitatively estimate the visible-light emission centers (VLECs) or energy states involved in the electronic transitions. The acceptor SLS (below the conduction band edge) are regarded as violet and blue VLECs, while the DLS are responsible for green, yellow, orange, and red VLECs [9].

PL spectra of $BaMoO_4$ were fitted with three Voigt area functions (VAFs) in allusion to specific VLECs. The deconvoluted PL spectra revealed that the green > blue > orange VLECs. The blue/-green emissions were correlated to acceptor SLS and DLS of intrinsic distorted $[MoO_4]$ clusters. In contrast, the orange emissions

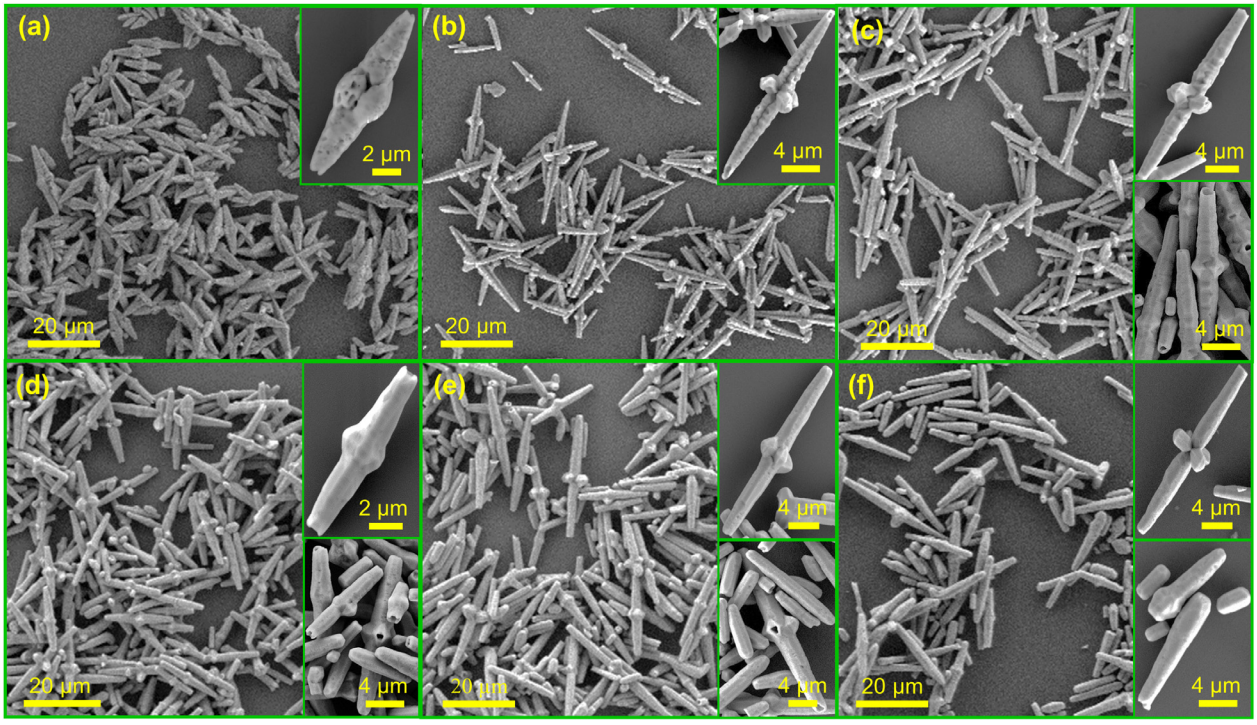

Fig. 1. SEM images of $BaMoO_4$ synthesized at 30 °C for 0 h (a) and 90 °C for 0 h (b), 2 h (c), 6 h (d), 12 h (e), and 24 h (f), respectively.

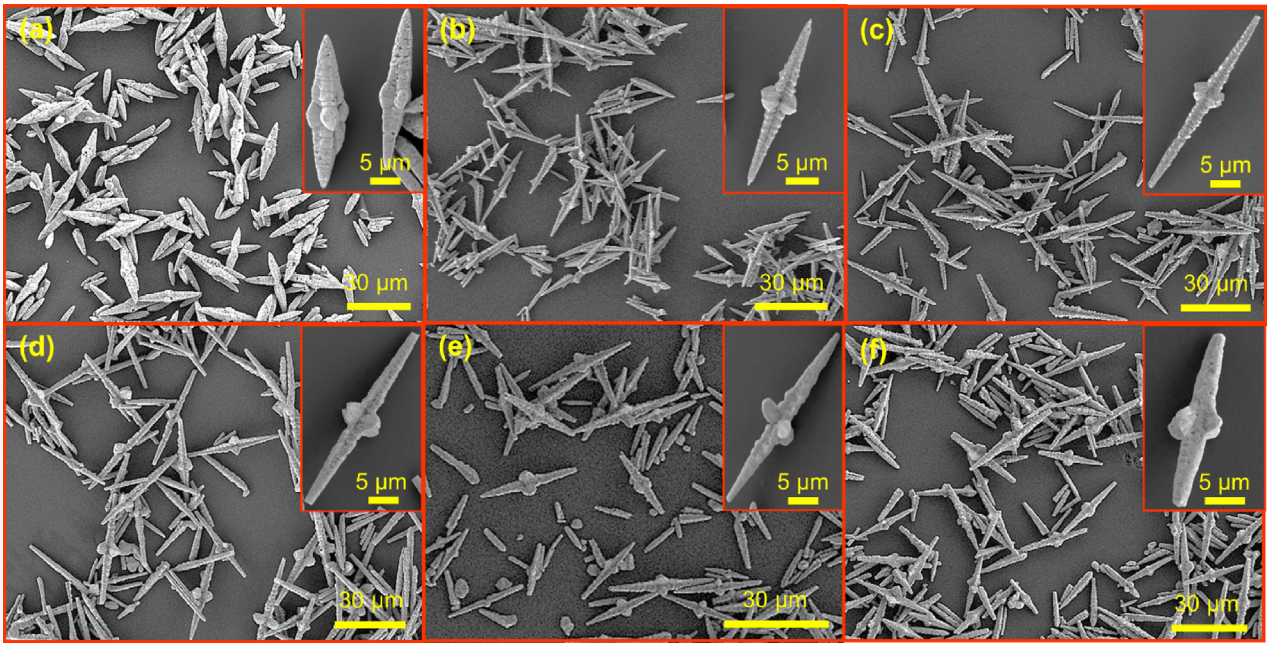

Fig. 2. SEM images of $BaWO_4$ synthesized at 30 °C for 0 h (a) and 90 °C for 0 h (b), 2 h (c), 6 h (d), 12 h (e), and 24 h (f), respectively.

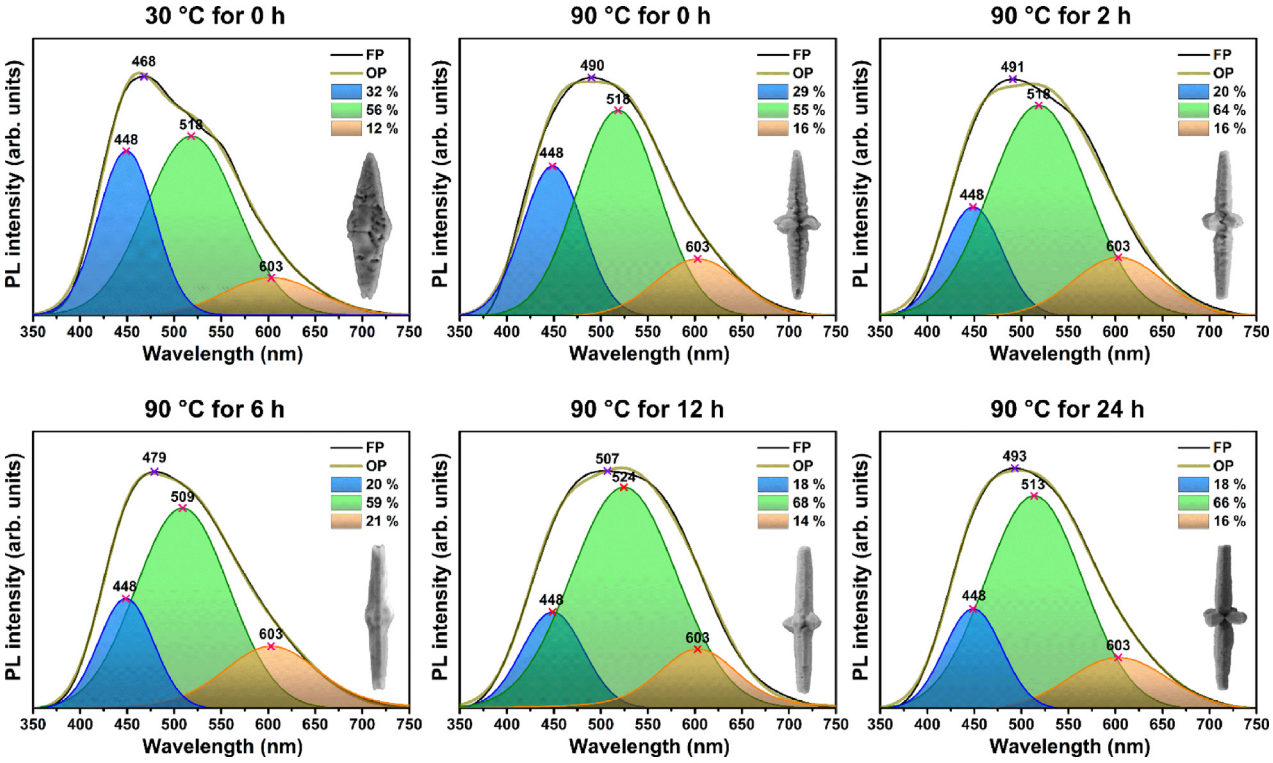

Fig. 3. Deconvoluted PL spectra of $BaMoO_4$ synthesized at 30 °C for 0 h, and 90 °C for different times.

were assigned to DLS originated by atomic displacements, dangling bonds, and bond distortions in $[BaO_8]$ – $[BaO_8]$ and/or $[BaO_8]$-– $[MoO_4]$ clusters [9].

Three or four VAFs were required to deconvolute the PL profiles of $BaWO_4$. The temporal evolution caused a pronounced redshift, indicating a change in the concentration and/or distribution of IEL in the band gap. Thus, there is majority participation of DLS (defects in $[BaO_8]$ – $[BaO_8]$ and/or $[BaO_8]$ – $[WO_4]$ clusters) concerning SLS (distorted $[WO_4]$ clusters). Although defects are often undesirable in phosphors, they were able to noticeably modify the PL emissions in $BaWO_4$. In particular, the PL properties of $BaWO_4$ were more affected by the experimental conditions than the $BaMoO_4$. Therefore, the band structure of $BaWO_4$ was more disturbed by the localized defect states.

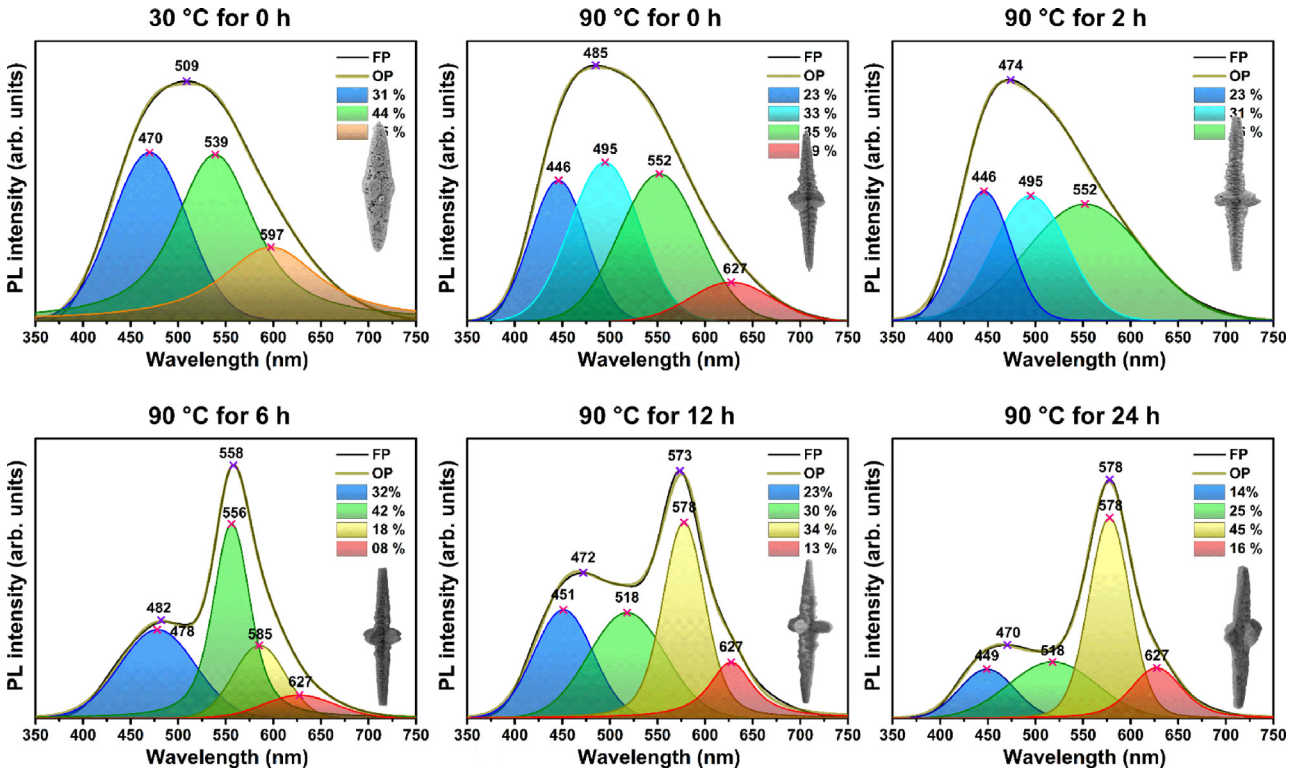

Fig. 4. Deconvoluted PL spectra of $BaWO_4$ synthesized at 30 °C for 0 h, and 90 °C for different times.

4. Conclusions

The results showed that both temperature and reaction time in P-FPI played a crucial role in the morphological control and optical properties of $BaMoO_4$ and $BaWO_4$. The defects created by the morphological changes affected both E_{gap} and PL emissions. This phenomenon was more prominent in $BaWO_4$, yielding red-shifted PL spectra as a function of the reaction times. These findings may offer a guidance for the design of phosphors with optimized optical properties for potential applications in electro-optical devices.

CRediT authorship contribution statement

Wyllamanney da S. Pereira: Conceptualization, Methodology, Visualization, Writing - original draft, Writing - review & editing. **Júlio C. Sczancoski:** Conceptualization, Methodology, Investigation, Project administration, Data curation, Validation, Visualization, Writing - original draft, Writing - review & editing. **Elson Longo:** Resources, Funding acquisition.

Declaration of Competing Interest

The authors declare that they have no known competing financial interests or personal relationships that could have appeared to influence the work reported in this paper.

Acknowledgments

We thank the CNPq (160355/2019-2), FAPESP (2015/11917-8; 2012/14004-5; 2013/07296-2), and CAPES for the financial support. Special thanks to Dr. Maximo Siu Li for the PL measurements.

Appendix A. Supplementary data

Supplementary data to this article can be found online at https://doi.org/10.1016/j.matlet.2021.129681.

References

[1] Y. Xu, Chapter 19 - Hierarchical Materials, in: R. Xu, Y. Xu (Eds.), Modern Inorganic Synthetic Chemistry (Second Edition), Elsevier, Amsterdam, 2017, pp. 545–574.
[2] Y. Yin, Z. Gan, Y. Sun, B. Zhou, X.u. Zhang, D. Zhang, P. Gao, Controlled synthesis and photoluminescence properties of $BaXO_4$ (X=W, Mo) hierarchical nanostructures via a facile solution route, Mater. Lett. 64 (6) (2010) 789–792.
[3] C. Shivakumara, R. Saraf, S. Behera, N. Dhananjaya, H. Nagabhushana, Synthesis of Eu^{3+}-activated $BaMoO_4$ phosphors and their Judd-Ofelt analysis: Applications in lasers and white LEDs, Spectrochim. Acta A 151 (2015) 141–148.
[4] D. Wang, K. Pan, Y. Qu, G. Wang, X. Yang, D. Wang, $BaWO_4$:Ln^{3+} Nanocrystals: Controllable Synthesis, Theoretical Investigation on the Substitution Site, and Bright Upconversion Luminescence as a Sensor for Glucose Detection, ACS Appl. Nano Mater. 1 (9) (2018) 4762–4770.
[5] A. Sahmi, S. Omeiri, K. Bensadok, M. Trari, Electrochemical properties of the scheelite $BaWO_4$ prepared by co-precipitation: Application to electro-photocatalysis of ibuprofen degradation, Mater. Sci. Semicond. Process. 91 (2019) 108–114.
[6] T.T. Basiev, A.A. Sobol, Y.K. Voronko, P.G. Zverev, Spontaneous Raman spectroscopy of tungstate and molybdate crystals for Raman lasers, Opt. Mater. 15 (3) (2000) 205–216.
[7] R.L. Penn, J.F. Banfield, Oriented attachment and growth, twinning, polytypism, and formation of metastable phases; insights from nanocrystalline TiO_2, Am. Mineral. 83 (9-10) (1998) 1077–1082.
[8] L. Tolvaj, K. Mitsui, D. Varga, Validity limits of Kubelka-Munk theory for DRIFT spectra of photodegraded solid wood, Wood Sci. Technol. 45 (1) (2011) 135–146.
[9] A.A.G. Santiago, C.R.R. Almeida, R.L. Tranquilin, R.M. Nascimento, C.A. Paskocimas, E. Longo, F.V. Motta, M.R.D. Bomio, Photoluminescent properties of the $Ba_{1-x}Zn_xMoO_4$ heterostructure obtained by ultrasonic spray pyrolysis, Ceram. Int. 44 (4) (2018) 3775–3786.
[10] M.D. McCluskey, E.E. Haller, Dopants and defects in semiconductors, CRC Press, Boca Raton, FL, 2012.